43rd Aerospace Science Meeting and Exhibit, January 9-13, Reno, Nevada

Computational Analysis of Laminar Boundary Layer Separation on a Slender Cone at Angle of Attack

Joseph Stecher* and Graham V. Candler**

Aerospace Engineering and Mechanics & Army HPC Research Center
University of Minnesota, Minneapolis MN 55455

Abstract

In this paper we compare the experimental results of a Mach 14.2 flow over a series of blunt cones at angle of attack with computational results of the same flow over the same cone. The experimental results come from a 1971 test by Stetson at the Aerospace Research Laboratories. The computational analysis was done with the Data Parallel Line Relaxation method. Surface pressure results on the leeward side of the cone, Pitot pressure surveys and surface streamlines all agreed with the experimental results. The computations under-predict the surface pressures on the wind side and in regions of strong cross flow for all cases. The source of this difference is unknown; several potential explanations are offered.

I. Introduction

Recently, there has been an increased interest in the development of a new class of lifting and maneuvering re-entry vehicles. An important concern for these vehicles is to accurately predict transition to turbulence along a flight trajectory. To address this need, an AFOSR and Sandia National Labs funded group is developing computational tools for mechanism-based analysis of flow stability and prediction of transition for re-entry vehicles. The STAR (stability and transition analysis for re-entry) effort is focused on the development and validation of a parabolized stability equations (PSE) solver for hypersonic boundary layers. This approach requires a very accurate laminar flow field to serve as the basis for the PSE analysis. Therefore, in support of the STAR program, it is necessary to assess and validate CFD methods for geometries similar to lifting re-entry vehicles at high Mach number and relevant angles of attack. Over thirty years ago Stetson performed a comprehensive study of the hypersonic flow over sharp and blunt cones at angle of attack.[1] Surface pressures, flow field Pitot pressure surveys, and surface oil flow visualizations were performed at a free-stream Mach number of 14.2 for a range of angles of attack up to 18°. This dataset is one of the few available for high Mach number lifting re-entry vehicle geometries; as such it could help validate CFD methods for accurate mean flow predictions for the STAR program.

These experiments were performed in the Aerospace Research Laboratory Mach 14.2 blowdown tunnel. The reservoir conditions of the Stetson experiments were 1600 psi (11.0 MPa) and 2050 °R (1140 K), resulting in a free-stream temperature of approximately 27.6 K and a total enthalpy of 1.15 MJ/kg. Clearly, this facility cannot provide validation data for high-temperature (real-gas) effects. But because this is a long duration facility (test times of over 5 minutes), careful surveys of the leeside flow field and surface separation / re-attachment patterns provide a wealth of data for CFD validation. Matching these data as well as the surface pressure measurements would provide confidence in the CFD methods and give guidance for grid resolution requirements for lifting re-entry vehicle flows. To our knowledge, a CFD analysis of this dataset has not been published.

* Graduate Research Assistant, AIAA Student Member (stecher@aem.umn.edu)
** Professor, AIAA Associate Fellow (candler@aem.umn.edu)

II. Stetson Mach 14.2 Experiments

The experiments were conducted in the Aerospace Research Laboratory (ARL) 20-inch Wind Tunnel at a nominal free-stream Mach number of 14.2 and Reynolds number of 2.0×10^6 per meter (0.62×10^6 per foot). The stated average test conditions in air were:

$$p_o = 1600\,\text{psi} = 11.02\,\text{MPa}$$
$$T_o = 2050\,^\circ R = 1140\,\text{K}$$
$$p_\infty = 0.0032\,\text{psi} = 22.06\,\text{Pa}$$
$$p_{\text{Pitot}\,\infty} = 0.85\,\text{psi} = 5860\,\text{Pa}$$

The wall temperature is quoted as approximately $0.29\,T_o = 330.3\,\text{K}$ for most of the experiments. An adiabatic flow gives $T_\infty = 27.56\,\text{K}$, and from $p_\infty = 0.0032\,\text{psi}$ (22.05 Pa), we obtain the free-stream conditions given in Table 1. However, if we use the given Pitot pressure of 0.85 psi (5860 Pa), we obtain a slightly different set of free-stream conditions, which are also given in Table 1.

The model consisted of a sting-mounted 5.6° half-angle cone with three different nose tips; a sharp tip (0.001″ radius) and nose radii of 10% and 30% of the cone base radius (equal to 1.5″). The model was instrumented with variable reluctance differential pressure transducers along a cone ray, with additional transducers for checking aerodynamic alignment. The stated accuracy of the surface pressure measurements is ±2% of the measured values.

The Pitot pressure surveys were performed with a 0.072″ OD tube; traverses were initiated on the model surface and then the probe was moved outward in the plane normal to the wind vector over a period of about three minutes. No attempt to correct for probe angle of attack was made. Surface oil flow visualizations were made using silicone oil painted on the model in longitudinal strips in the windward region and circumferential strips in the leeward region. Stetson's original photographs of the oil flows were digitally scanned by Prof. Steven Schneider of Purdue University.

We undertook a CFD analysis of the ARL nozzle flow to provide a new estimate of the operating conditions. We used the approach discussed in Ref. 2; in this case the effects of vibrational nonequilibrium are minimal, however the gas is thermally imperfect at the reservoir conditions. Therefore we used an excluded volume equation of state[3,4] for high pressure air

$$p = \frac{\rho R T}{(1 - b\rho)}$$

where R is the gas constant for air and b is a correction for the volume excluded by the air molecules. We use $b = 0.001024\,\text{m}^3/\text{kg}$.

We do not have the nozzle contour details for the ARL tunnel. However, the computed conditions are insensitive to the nozzle geometry provided that there are no strong compression waves in the nozzle flow. We therefore used the NSWC/AEDC Tunnel 9 Mach 14 contour available from the literature.[5] We then used our CFD code to expand the flow from the given reservoir conditions to the measured Pitot pressure of 0.85 psi (5860 Pa). This results in a third set of free-stream conditions, which are given in Table 1.

TABLE 1. Wind-tunnel free-stream conditions.

	Nominal 1[a]	Nominal 2[b]	Computed
M_∞	14.20	14.20	14.52
T_∞ (K)	27.56	27.56	27.47
ρ_∞ (g/m^3)	2.788	2.847	2.721
u_∞ (m/s)	1495	1495	1526
p_∞ (Pa)	22.06	22.53	21.46
$p_{\text{Pitot}\,\infty}$ (Pa)	5740	5860	5860

[a]Using given static pressure

[b]Using given Pitot pressure

III. Computational Method

We used the NASA Ames Data-Parallel Line-Relaxation (DPLR) code[6] to simulate the Stetson experiments. The DPLR code uses the second or third-order accurate flux evaluations and a parallelized implicit time integration method to allow solutions to be obtained efficiently.

We generated the grid using the commercially-available Gridgen program. The mesh used in the simulations is divided into two blocks; the first block is a nose patch of $48\times96\times150$ points, and the second block represents the remainder of the geometry with $248\times193\times150$ points. Because of the symmetry of the problem, we only modeled half of the cone. Figure 1 shows the grid used for the 30% blunt cone, with the grid optimized for a 10° angle of attack. Because separation occurs on the leeward side of the cone, we clustered points in that region. For the 0° angle of attack case, we used a 2-D grid in order to reduce computation time.

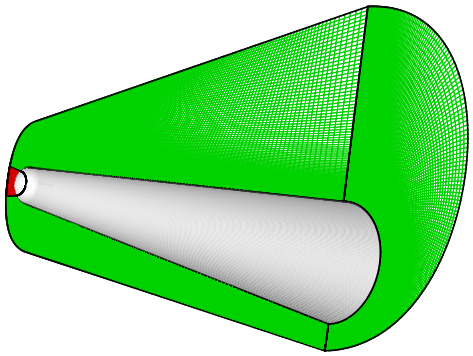

FIGURE 1. **30% blunt cone model and grid optimized for 10° angle of attack, showing the grid on the exit and symmetry planes.**

As explained in the discussion section, for both the axisymmetric and 3-D cases, various grid resolutions were tried in order to evaluate grid performance. Computational runs were performed with increased grid resolution in each coordinate direction. Additionally, for the 3-D case, different clustering methods were attempted to improve model performance. It should be noted that the baseline grid has 7.87×10^6 grid points, which is a large grid for this relatively low Reynolds number flow. y^+ values were calculated for the first grid in the wall-normal direction for both the 10% and 30% blunt cases. In both cases, y^+ values were less than unity.

IV. Computational Results

We simulated the 10% and 30% blunt cones at a range of angle of attack up to 10°. Longitudinal and circumferential surface pressures and Pitot pressure surveys were compared with the experimental data. In addition, we visualized the near-surface velocity field to compare with the oil flow measurements presented by Stetson.

Table 1 presents three possible free-stream conditions for the experiment. We computed the 30% blunt, $\alpha = 10°$ case with each condition, and found only very small differences in the longitudinal pressure distribution. Therefore, we used the conditions given as Nominal 2; these are obtained using an adiabatic, isentropic expansion from the reservoir conditions to the measured Pitot pressure. However, we normalized the pressure distributions by the free-stream pressure given by Stetson of 0.0032 psi = 22.05 Pa. This is slightly different than our free-stream pressure, however the Stetson's data were normalized by this value. (Table 1 shows that this difference in p_∞ is small.) In all cases, unless otherwise stated, we used a wall temperature of 330.3 K for the entire cone surface.

First consider the longitudinal pressure distributions for the 30% blunt cone shown in Fig. 2. The first plot shows the pressure distribution for the axisymmetric case. Note that the isothermal wall simulation under predicts the pressure distribution, particularly near the nose. To assess the effect of wall temperature, we also ran an adiabatic wall condition; this shows better agreement for most of the cone, with a slight under prediction near the nose. It is unlikely that the cone surface would reach the adiabatic limit during the test. Stetson performed some runs where the model was heated to a temperature of 417 K during a 5 minute run; this is substantially lower than the adiabatic wall temperature of 994 K at $X/R_n = 10.0$. Therefore, the improved agreement due to the adiabatic wall is almost certainly spurious.

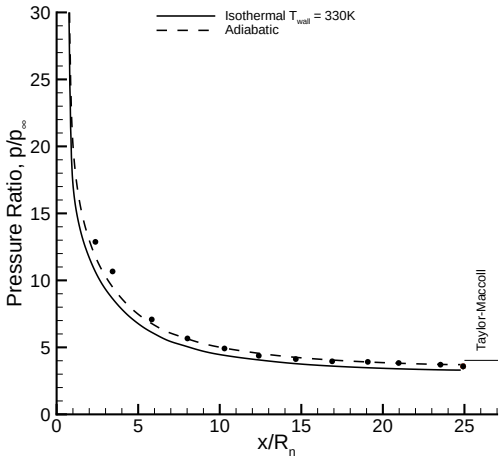

(a) $\alpha = 0°$

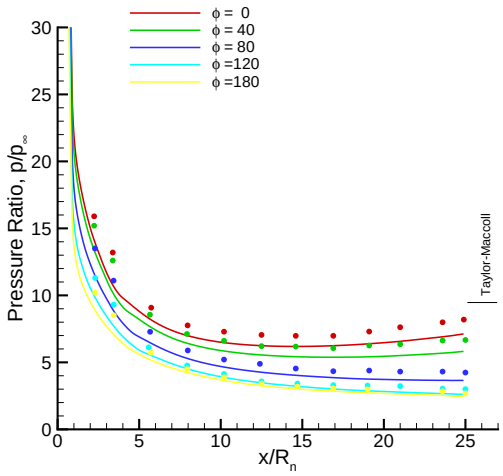

(b) $\alpha = 4°$

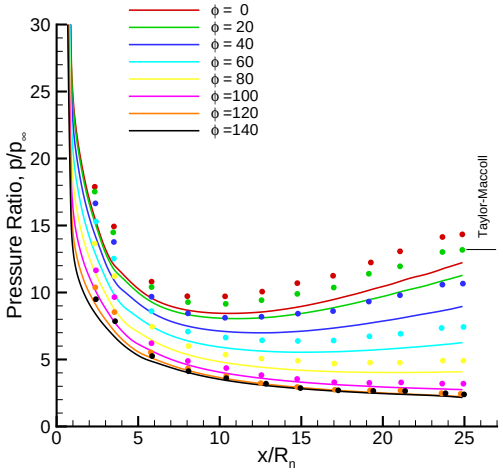

(c) $\alpha = 6°$

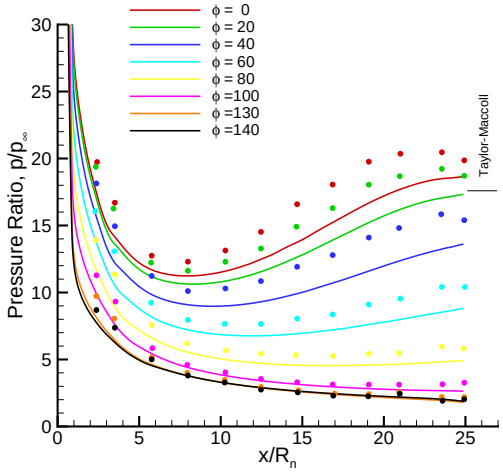

(d) $\alpha = 8°$

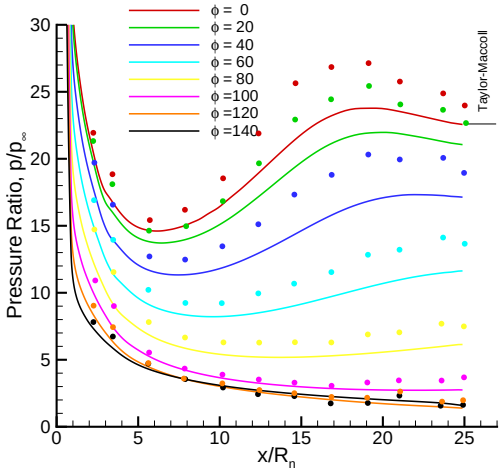

(e) $\alpha = 10°$

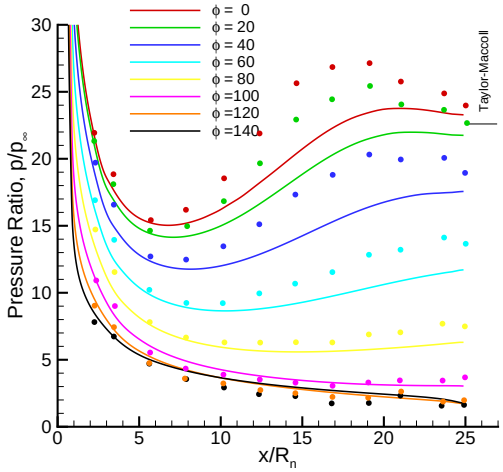

(f) $\alpha = 10°$ **adiabatic wall**

FIGURE 2. **Longitudinal surface pressure distributions for the 30% blunt cone.** ϕ **denotes the circumferential angle from the windward side.**

Now consider the remainder of Fig. 2, which shows the longitudinal pressure distributions for angles of attack up to 10°. In these plots, $\phi = 0°$ is the windward side and $\phi = 180°$ is the leeward side of the cone. In general, the computational results under-predict the pressure distributions, and overall the agreement is rather poor. Some details stand out in these plots:

1. The computations predict the general trend with a substantial over-expansion on the windward side, followed by a re-compression.
2. The windward side agreement gets worse with increasing angle of attack.
3. The pressure distributions for circumferential angles with substantial cross flow ($\phi = 40, 60, 80°$ are also poorly predicted. In most cases, the relative error is larger than on the windward side.
4. The leeward side pressure ($\phi \geq 120°$) is well predicted for all cases.

We also ran the $\alpha = 10°$ case with an adiabatic surface condition; Fig. 2 (f) shows that the agreement is worse than the isothermal wall case. The peak in the windward pressure is moved further downstream, and the leeside pressure is now over-predicted. Thus, it is highly unlikely that wall temperature uncertainties are the cause of the poor agreement.

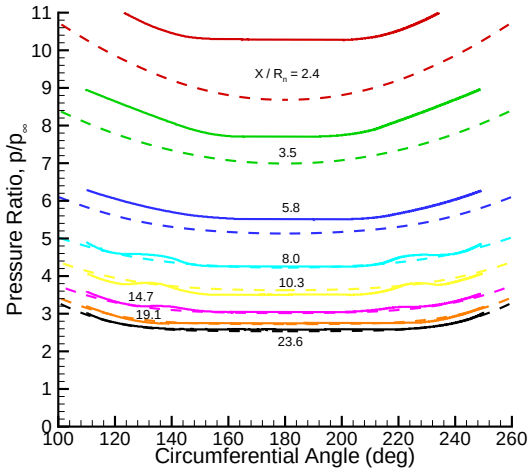

(a) $\alpha = 4°$

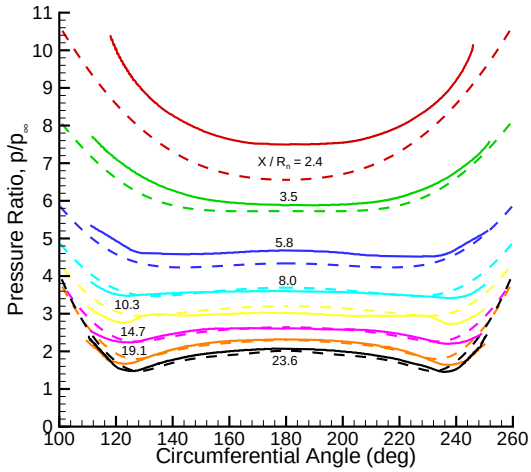

(b) $\alpha = 6°$

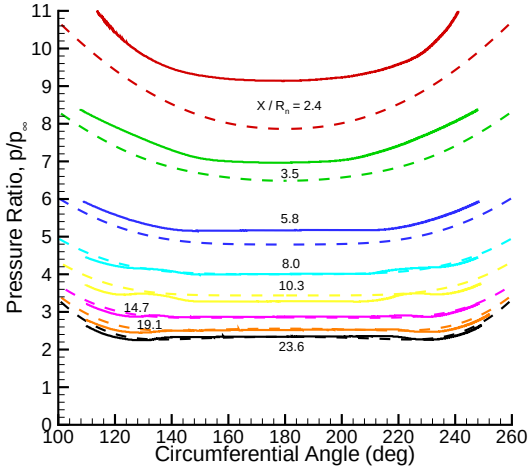

(c) $\alpha = 8°$

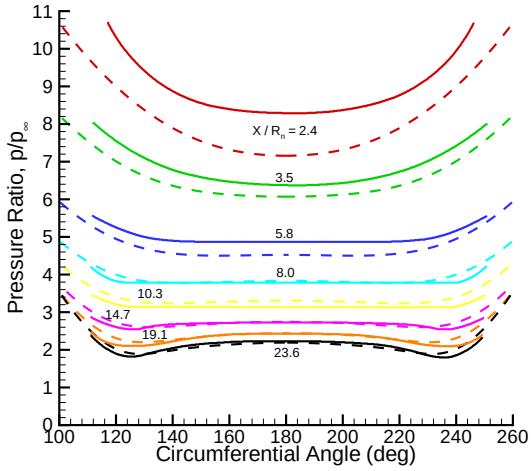

(d) $\alpha = 10°$

FIGURE 3. **Circumferential pressure distributions at constant X/R_n locations. Solid lines: Stetson[1]; dashed lines: present results.**

Also shown on the plots in Fig. 2 is the pressure obtained from solving the Taylor-Maccoll equations[7] for conical flow. Note the excellent agreement for the $\alpha = 0°$ case; a slight over-prediction of the theoretical result is expected due to boundary layer displacement. For the non-zero angle of attack cases, the Taylor-Maccoll values are approximate, but in general they agree better with the computational results than the experiments. Newtonian aerodynamics predicts slightly lower values than the Taylor-Maccoll equations, again in better agreement with the computational results.

Stetson also made detailed surface pressure measurements for circumferential angles near the leeward plane of symmetry. Fig. 3 compares the computations (dashed lines) and experiments (solid lines) for four angles of attack at various axial locations on the cone. Note the excellent agreement in the regions of low pressure near the leeward centerline for the aft portion of the cone.

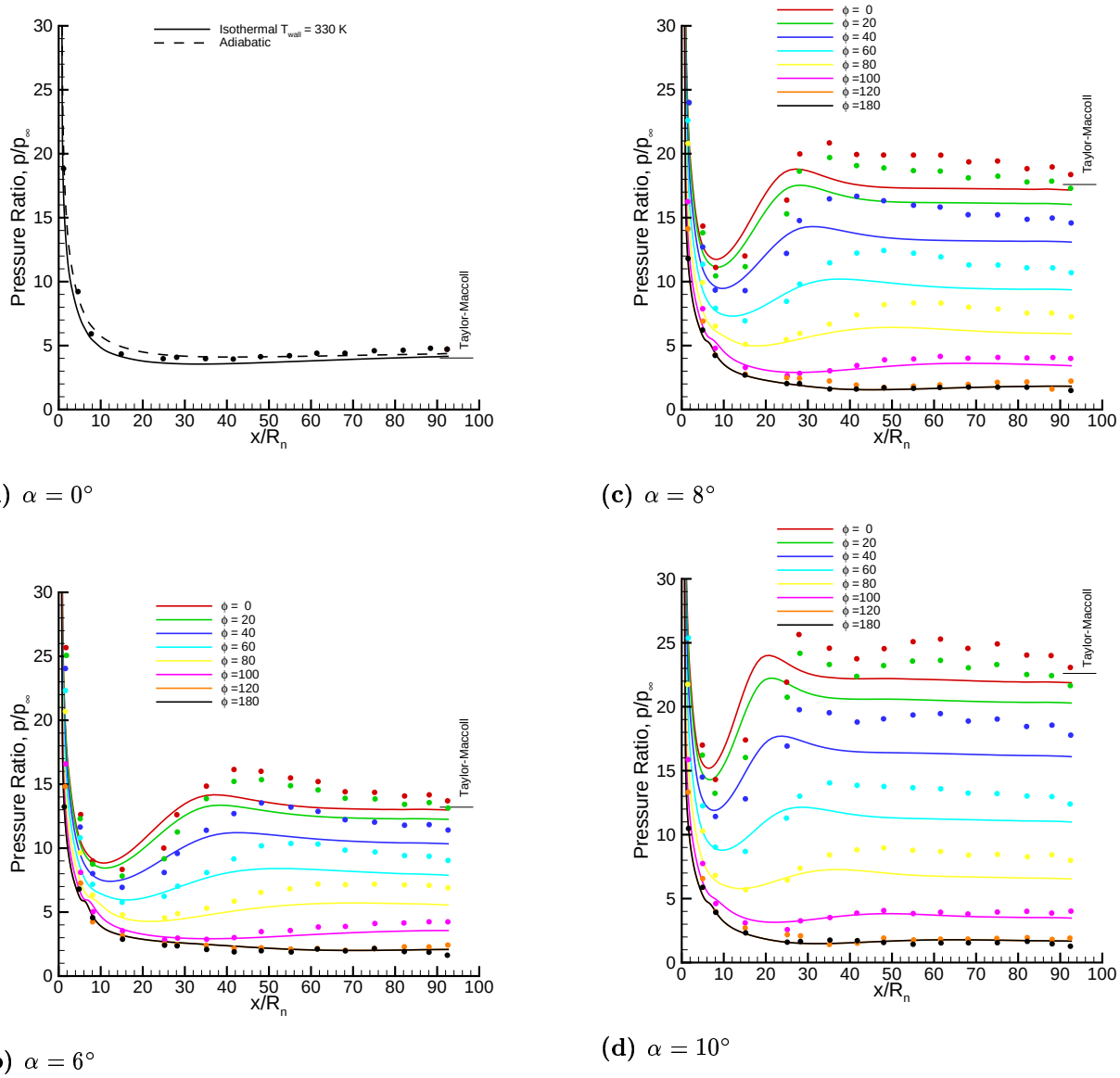

(a) $\alpha = 0°$

(c) $\alpha = 8°$

(b) $\alpha = 6°$

(d) $\alpha = 10°$

FIGURE 4. **Longitudinal surface pressure distributions for the 10% blunt cone.**

Figure 4 plots the longitudinal pressure distributions for the 10% blunt cone; the results are quite similar to the 30% blunt case. Now because of the smaller bluntness, the pressure distributions become nearly constant on the aft section of the cone. Again, in general the leeward side pressures are correctly predicted, and the remainder of the pressure field is under-predicted. There is notably poor agreement for the $\alpha = 10°$ case for $\phi \leq 80°$.

We also ran a case at $\alpha = 10.5°$ to assess the sensitivity of the pressure distribution to a possible error in the angle of attack. We found that in order to match the windward pressure, the leeward pressure distribution is corrupted. Therefore, this is not a possible source of error.

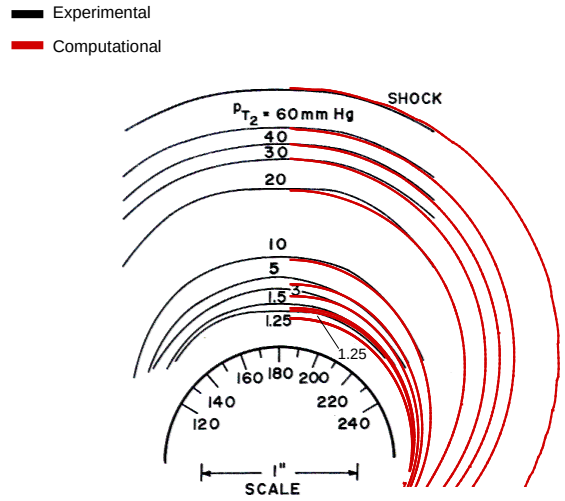

(a) $\mathbf{X}/R_n = 8.0$

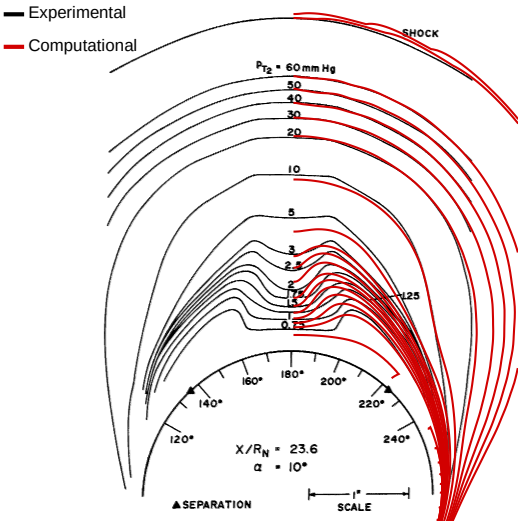

(c) $\mathbf{X}/R_n = 23.6$

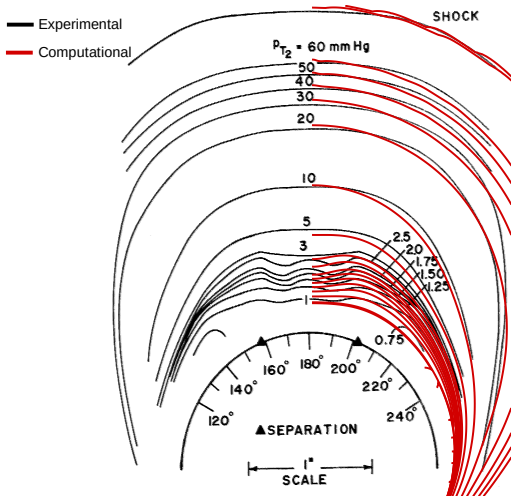

(b) X/ $R_n = 14.7$

FIGURE 5. **Pitot pressure surveys for the 30% blunt cone at 10° angle of attack**

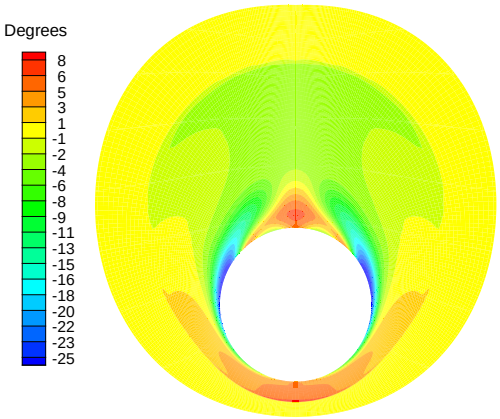

FIGURE 6. **Flow angle relative to freestream at $\mathbf{X}/R_n$=23.6 for the 30% blunt case at 10° angle of attack**

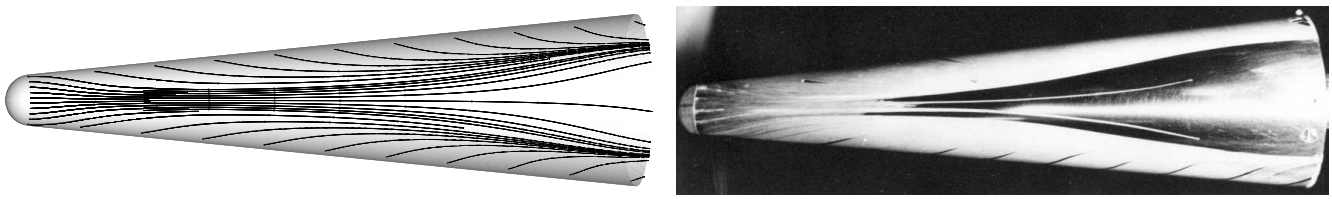

(a) 30% bluntness, $\alpha = 10°$

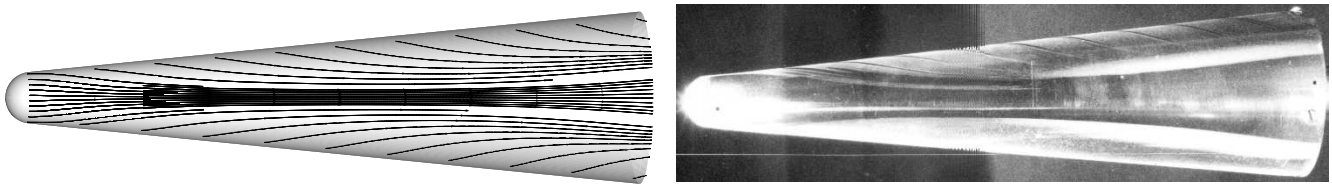

(b) 30% bluntness, $\alpha = 8°$

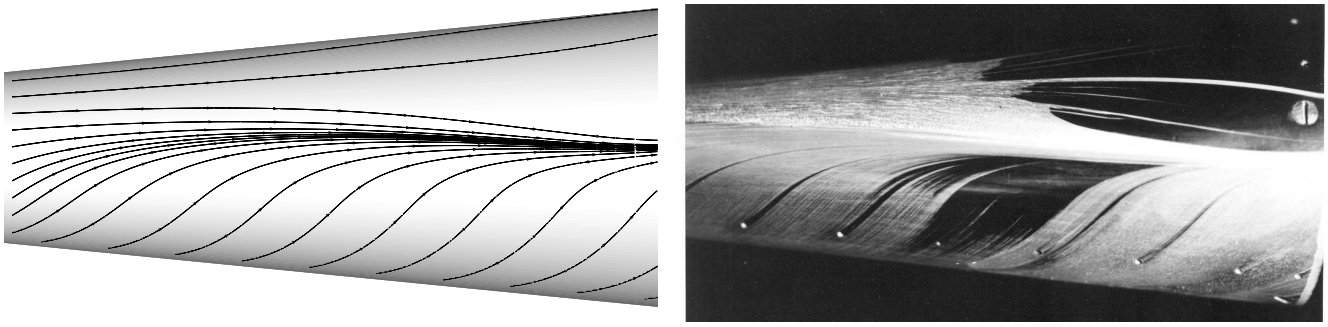

(c) 30% bluntness, $\alpha = 10°$

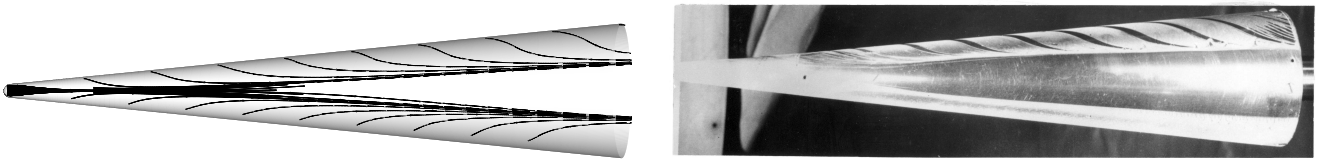

(d) 10% bluntness, $\alpha = 8°$

FIGURE 7. **Computed surface streamlines and experimental oil flow photographs for various cases.**

In addition to longitudinal and circumferential pressure distributions, Stetson provides several Pitot pressure surveys in the leeward region of the 30% blunt cone at 10° angle of attack. Figure 5 presents the original plots with the simulations superimposed. It should be noted that the location of the model in the original plots is misleading. The plane is perpendicular to the free-stream velocity vector, and therefore the cross-section of the cone should be elliptical, rather than circular as shown. This accounts for the lack of Pitot pressure contours near the upper surface of the model. In any case, the comparisons are relatively good, with the majority of the Pitot contours overlaying the experiments. The main discrepancy is in the low pressure region where the flow field is very complicated due to separation and boundary layer lifting.

There is an additional concern in this region due to flow angularity potentially reducing the accuracy of the Pitot pressure probe. Figure 6 plots the flow angle relative to the free-stream velocity vector for the $X/R_n = 23.6$ plane. Note that much of the flow where there is relatively poor agreement coincides with the high flow angularity.

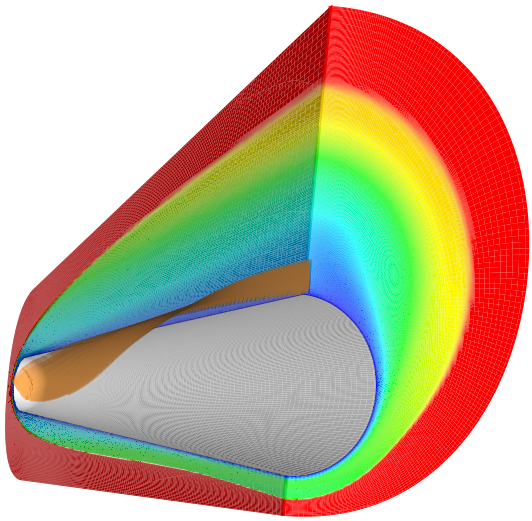

FIGURE 8. **30% blunt cone at 10° angle of attack with Mach contours on symmetry and exit planes and stream ribbon for flow visualization.**

The final figures are visualizations of the 30% blunt cone flow field at $\alpha = 10°$. First consider Fig. 7, which plots the computed and measured surface flow patterns for several cases. For the computations, the near-surface flow is visualized by tracing streamlines in the wall-normal plane closest to the model surface. For the experiments, the flow is visualized with silicone oil painted onto the model surface prior to the run. Note the strong similarities between the visualizations; the flow appears to separate at the same locations and the rapid streamline curvature prior to separation is strikingly similar (especially in contrast to the poor surface pressure agreement).

The final plot shows the Mach number contours in the plane of symmetry and the flow exit plane for the 30% blunt cone. Also plotted are stream ribbons to visualize the separated flow on the leeward side.

V. Discussion

These results are puzzling. *A priori* we would have expected the windward pressures to be predicted very accurately, and any differences would show up in the leeward pressures. However, exactly the opposite is the case. Other than this being somehow related to the "joy of research," it is disconcerting.

There are several possibilities for this discrepancy between the computed and experimental results:

1. There is something wrong with the DPLR code that incorrectly predicts the pressure.
2. The grid is under resolved or defective in some other way.
3. There was an error introduced into the original measurements of the flow.

The first item is exceedingly unlikely. DPLR has been tested and experimentally verified on much more complex flows than a simple blunt cone. A double-cone experiment with chemically reacting flows has been experimentally verified with DPLR[2]. This simple, non-reacting flow should be well within the capabilities of this code.

The second item, while more likely than the first, has also been systematically eliminated from possibility. As stated in section III., the grid has 7.87×10^6 points in it, which is large for such a simple geometry and flow. Even with that large number of points, several runs were attempted with even larger numbers of points. We found that increasing the number of points did not improve results in either the 2-D or the 3-D cases. Various clustering schemes were tried, and clustering toward the leeward plane of symmetry was found to marginally improve results. Additionally, the y^+ values were calculated for the first grid in the wall-normal direction for

both the 10% and 30% cases. In both cases, y^+ values were less than unity. This indicates that the grid should be of sufficient quality to accurately predict this flow.

In discussing the third possibility, it is useful to make a comparison with some idealized flow theories. This will quantify which set of data has more of a discrepancy relative to theory. Table 2 shows the pressure at $X/R_n = 92.5$ on the windward side of the cone for the 10% blunt case at 10° angle of attack. In addition to Stetson's data and our computed data, we evaluated what Newtonian theory and the Taylor-Maccoll equation predict for pressure at that location. A review of the literature indicates that we are the first group to calculate the windward side of this flow. Lubard[8] computed the leeward side of the flow, but not the windward. Therefore we have no other computational data with which to compare our results against. This means we must compare with theory and the data set that we are given by Stetson.

The data in the table indicate that our computed result is larger than Newtonian theory, but agrees well with the Taylor-Maccoll predicted result. Newtonian theory is consistently lower than both the Taylor-Maccoll predicted pressure and the computed pressure. The experimentally derived pressure is also consistently higher than both our computed results and what the Taylor-Maccoll equation would predict. We would expect for the 10% blunt cone, both the computed case and the experimental case would approximate the Taylor-Maccoll derived pressure. The Taylor-Maccoll equation assumes a semi-infinite cone, and in the case of the 10% blunt cone, the cone is long enough for this assumption to be valid. We can confirm this in figure 4. We would expect the pressure to be near that of the Taylor-Maccoll derived pressure, which figure 4 shows.

TABLE 2. Normalized surface pressure on 10% cone at $x/R_n = 92.5$. Note that for the purposes of this table, the computed and measured values have been normalized by the free-stream pressure corresponding to Nominal 2 conditions in Table 1.

α (deg)	Newtonian	Taylor-Maccoll	Stetson	Computed
0	3.69	4.03	4.82	4.24
6	12.41	13.20	14.01	13.27
8	16.61	17.59	18.79	17.52
10	21.42	22.61	23.59	22.35

The consistency with which our computed results match the Taylor Maccoll predicted results would further lead us to believe that our computed results are correct. Therefore, we must explore the possibility something was overlooked in the measurement of the original data set. The freestream pressure for this flow is about 22 Pa, an extremely low pressure to achieve, let alone measure.

The low pressures involved mean that the method used to measure that pressure is very important. Stetson states that pressure is measured through a series of ports on the surface of the cone. These ports are relatively large, on the order of .05″ in diameter, or 1.6% of the cone base diameter. The ports are connected to tubes which run down the center of the sting for an unknown length and into the pressure transducer. Previous pressure measurements of a similar nature done by Holden[10] on low density hollow cylinder flares were improved by the use of flush mounted pressure sensors.

On the windward side of the cone, as angle of attack increases, there will be a strong shear, and the boundary layer will become thinner. This thin, high shear boundary layer could possibly catch in the rather large openings of the pressure taps. If even a small amount of high velocity flow is captured by the pressure taps, this could potentially cause the discrepancy between the two data sets that we are seeing. The δ_{99} boundary layer thickness at $X/R_n = 23.6$ on the 30% cone at 10° angle of attack is 0.125″ or 3 mm, which is about 2.5 pressure port diameters. The freestream velocity behind the shock is about 1475 m/s. At 1 pressure port diameter away from the surface, the flow speed is about 1250 m/s. We can see that there is ample high speed flow close to the surface that could be captured by the pressure port.

The angle of attack of the vehicle and the resulting thin shear layer being captured by the pressure tap may account for the discrepancy between our computational result and the experimental results achieved by Stetson. We believe that given the technology available at the time, and the difficulty of making measurements of a high speed low pressure flow, this discrepancy was unavoidable.

VII. Conclusions

We performed a systematic CFD study of the dataset from Stetson for laminar flows over blunted cones at angle of attack. We used a well-established CFD method with a fine grid for 10% and 30% blunt cones at a range of angles of attack up to 10°. We found that the simulations predict the lee side surface pressure, oil flow, and Pitot pressure fields very well. However, the comparison is poor for the wind side pressure distribution, and for regions where there is strong cross flow. We confirmed that the solutions are grid resolved, and we found that the wall temperature boundary condition affects the results, but cannot explain the discrepancy. Our computations are in close agreement with Newtonian and Taylor-Maccoll theory. Therefore, there is some concern about the accuracy of the wind side surface pressure data. However, the good agreement with the lee side measurements is encouraging because this part of the flow field is challenging to simulate because of the complex vortical separated flow.

VIII. Acknowledgments

This research is supported by Air Force Office of Scientific Research (AFSOR) under Grant F9550-04-1-0341. The views and conclusions contained herein are those of the authors and should not be interpreted as necessarily representing the official policies or endorsements, either expressed or implied, of the AFSOR or the U.S. Government. This work was also supported by Sandia National Laboratories, under contract 80377. We would also like to thank Dr. Steve Schneider for his assistance in scanning the original oil flow photographs used in this work. We would also like to thank Mr. Kenneth Stetson for helpful discussions concerning his experiments.

IX. References

[1] Stetson, K.F., "Experimental Results of Laminar Boundary Layer Separation on a Slender Cone at Angle of Attack at $M_\infty = 14.2$," Aerospace Research Laboratories, ARL 71-0127, Aug. 1971.

[2] Nompelis, I., G.V. Candler, and M.S. Holden, "Effect of Vibrational Nonequilibrium on Hypersonic Double-Cone Experiments," *AIAA Journal,* Vol. 41, No. 11, pp. 2162-2169, Nov. 2003.

[3] Lordi, J.A., and R.E. Mates, "Nonequilibrium Expansions of High-Enthalpy Flows," Aerospace Research Laboratories, ARL 64-206, Nov. 1964.

[4] Thompson, P.A., *Compressible-Fluid Dynamics,* McGraw-Hill, NY 1971, pp. 95-102.

[5] Korte, J.J., E. Hedlund, and S. Anandakrishnan, "A Comparison of Experimental Data With CFD For NSWC Hypervelocity Wind Tunnel 9 Mach 14 Nozzle," AIAA Paper 92-4010, July 1992.

[6] Wright, M.J., D. Bose, and G.V. Candler, "A Data-Parallel Line Relaxation Method for the Navier-Stokes Equations," *AIAA Journal,* Vol. 36, No. 9, pp. 1603-1609, Sept. 1998.

[7] Taylor, G.I., J. W. Maccoll, "The Air Pressure on a Cone Moving at High Speeds," *Proceedings of the Royal Society of London,* Vol. 139, No. 838, pp. 278-297, Feb. 1933.

[8] Lubard, S.C., and W.S. Helliwell, "Calculation of the Flow on a Cone at High Angle of Attack," AIAA Paper No. 73-636, July 1973.

[9] M. Holden, T. Wadhams, J. Harvey, G. Candler, "Experiments and DSMC and Navier-Stokes Computations for Hypersonic Shock Boundary Layer Interactions" AIAA Paper No. 2003-1131, Jan. 2003